Lasers in Manufacturing Conference 2015

Development of an adaptive focus position control system for a new high-performance laser remote welding head

G. Cerwenka[a,*], J. Wollnack[b], C. Emmelmann[a]

[a]*Hamburg University of Technology (TUHH), Institute of Laser and System Technologies (iLAS), Denickestr. 17, D-21073 Hamburg, Germany*
[b]*Hamburg University of Technology (TUHH), Institute of Production Management and Technology (IPMT), Denickestr. 17, D-21073 Hamburg, Germany*

Abstract

The Institute of Laser and System Technologies (iLAS) of the Hamburg University of Technology (TUHH) investigated an intelligent vision guided laser remote scanner (LRS) system not only for thin sheet or structure applications, but also for thick sheet welding tasks with brilliant high power lasers up to 30 kw optical laser power. Two different wavelength acting; 532 nm for measuring and analyzing processes, 1070 nm for welding and other laser processes. Mechanical, thermal and optical effects mainly influence the manufacturing results after position, shape and machining path measuring processes. Especially the high laser power induced interaction between the laser beam and optical components will change the optical guidance properties in the course of time. Changing the refraction index n is one of the important effects for the thermo-optical reaction; focal shift takes place. The conclusion is now, that the machining position of an infrared high power laser spot does not fit anymore to the measured and analyzed position of the green pointing laser spot. The paper describes a first basic simulation model of the optics from this new LRS system with influencing components and important parameters. Furthermore the thermal influences have been simulated and the first results are presented. These results demonstrate the importance to develop within the next steps a combined practical and fast correction algorithm design supported by real sensor signals and implemented in the laser remote scanner controller unit.

Keywords: laser remote technology, scanner technology, laser remote scanner, laser remote welding, high power laser, focus shift, thermal lense, system technology, process monitoring and control, simulation, joining, welding, brazing

* Corresponding author. Tel.: +49 (0)40 484010 632; fax: +49 (0)40 484010 999.
Email address: georg.cerwenka@tuhh.de.

1. Introduction

1.1. Laser remote welding

In addition to robot-guided, short-focus laser welding processes in industrial applications increasingly long-focus laser welding processes are used, but invariably in thin sheets. As a leading industry, the automotive industry is to be mentioned [1, 2, 3, 4]. The system distinction consists in length of the working distance, i.e. distance between focusing lens and processing position. Compared to laser welding with focal lengths below $300\ mm$ typical working distances $> 300\ mm$ to currently $1600\ mm$ are called laser remote welding (LRW) processes [5, 6]. A limitation of theoretical feasible working distances and possible focal lengths is determined only by the quality of the laser beam respectively by the brilliance of used laser system, by the optics system and by the process required intensity distribution at the working area [7].

The Institute of Laser and System Technologies (iLAS) explores for several years already possibilities, limitations and appropriate use cases for LRW [8, 9, 10, 11, 12]. The results confirm that the use of the method is particularly suitable for manufacturing tasks with high non-productive times, caused by complex repositioning. In the automotive industry the duty cycle time for the laser could be increased from $30\ \%$ to approximately $90\ \%$ [10, 13].

1.2. High-performance laser remote welding head

In the BMWi-funded joint research project QuInLas (2010 – 2014) the laser remote technology was initially introduced by the iLAS to shipbuilding industry [11]. For shipbuilding applications with respect to material thickness adapted beam qualities and outputs an intelligent vision guided high-performance LRW system has been investigated for thin and thick sheet welding tasks with brilliant high power lasers up to $30\ kW$ optical laser power [12, 14]. Due to the characteristic circumstances, the working distance could be expanded to approximately $1\ m$ using an $30\ kW$ optical laser power IPG laser source, which was newly developed during the project. However it is still possible to join plate thicknesses of $10\ mm$ by the deep welding effect. A multi-camera based position and shape detection system with laser-based measuring spot for direct analysis of component location and automated determination of machining contour was implemented in the new built-in function concept of the LRS head [12, 15, 16]. Two different wavelength acting; $532\ nm$ for measuring and analyzing processes, $1070\ nm$ for welding and other laser processes [17].

However, so far no of this LRS systems are utilized for determination of the position and for shape measurement as well as for joining of parts and assemblies for high power applications. Mechanical, thermal and optical effects mainly influence the manufacturing results after position, shape and machining path measuring processes. Especially the high laser power induced interaction between the laser beam and optical components will change the optical guidance properties in the course of time. Currently there are no practicable and temperature stabilized ways to track the focus position for high-performance laser remote scanner systems during measurement and joining process.

2. Thermal effects

Differently induced influences evoke thermal effects throughout the complete LRS head and affect the thermal stability. These factors mainly include the direct rise of temperature in the lenses and the laser-safe, enclosed housing by absorbed laser radiation and by heat generation of electronic components as well as the

changes of temperature in the vicinity. The materials and material compounds used for the construction react to changes in temperature with an expansion or contraction in accordance to their substance-specific material constant differently. This specific change is represented by means of the thermal expansion coefficient α for a linear expansion respectively γ for a spatial expansion [18, 19]. However, materials generally do not stretch uniformly over the entire temperature range. For this reason the thermal expansion coefficient itself is temperature-dependent and only meaningful in relation to a reference temperature or a defined temperature range. The general formulas for both expansion coefficients are [18, 19]:

$$\alpha = \frac{1}{L_0} \cdot \frac{dL}{dT} \tag{1}$$

$$\gamma = \frac{1}{V_0} \cdot \left(\frac{\partial V}{\partial T}\right)_{p,N} \tag{2}$$

Thereby L_0 is the length and V_0 the volume at a defined reference temperature T_0. The differential or partial derivatives dL/dT and $\partial V/\partial T$ symbolize the respective change of the quantity. In case of spatial expansion, the two indices characterizing the pressure p and the number of particles N in the volume V_0 and shall be held constant for the determination of γ. These two equations show that a change of the temperature causes also a change of component location relations, previously defined positions and reference coordinates and can lead to measurement and processing variations.

The entire thermally induced focus position shift is made up of all changes in the individual components, such as the fiber connector, the collimating and focusing lenses to the deflecting mirrors and the protective glass [20]. The laser-induced thermal change of the lens material causes optical aberrations [21]. Depending on the lens material used the absorption in the material per path length is $10^{-3}\ m^{-1}$ to $10^{-6}\ m^{-1}$ [22]. Lenses in optical systems are commonly adopted in a fixture. It occur the mechanisms of heating and cooling shown in figure 1.

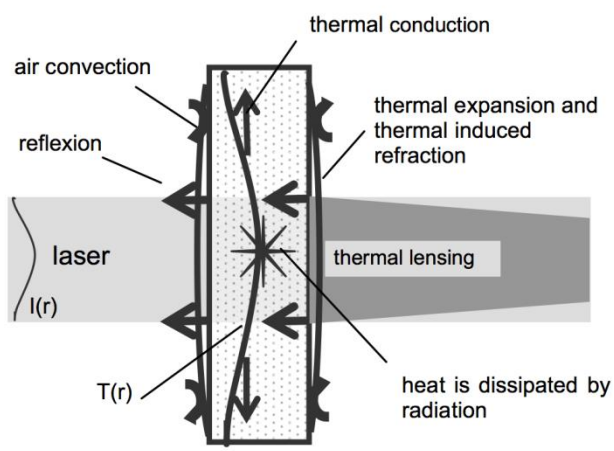

Figure 1: Thermal interaction of the laser beam with an optical element, $\mathrm{I(r)}$ … intensity distribution of the laser beam, $\mathrm{T(r)}$ … radial temperature profile within the lens [22]

For the most part the physical effect of heat conduction carries heat away from the center of optical elements to the edge. With a correspondingly high heating of the lens material an additional effect of free convection emerges intensified. If the temperatures reach in the center of an optical element several hundred degrees, the radiation cooling makes a significant contribution. These effects influence the temperature gradient within the optical element, which has a direct effect on the optical beam path during the propagation through the optical element [22].

The shift of the focus position along the propagation is described in the literature as thermally induced focus shift [7]. Often the most intense for the thermo-optical effect causes the change of the refractive index n. The result is a significant focus shift. Experimental studies of Wolf et al., 2009 at an industrial set up of a fiber-coupled singlemode laser system showed already for an optical laser power of $1\ kW$ and a beam waist diameter of $60\ \mu m$ in focus at a power increase of $10\ \%$ to $100\ \%$ a significant focus shift of approximately $25\ mm$ with an associated beam waist widened to a factor of 4 [23]. Reitemeyer et al., 2009 obtained similar results for a fiber-guided multimode laser system at $7\ kW$ optical laser power and a beam waist diameter of $100\ \mu m$ [24]. The focus shift is approximately $70\ \%$ of the Rayleigh length with an increase of the laser power to $7\ kW$. However the beam diameter change is lower and amounts to only $2\ \%$ [24]. Nevertheless there was a change in the intensity distribution after a not unusual, beam emitting duty cycle of $60\ s$. The initial top-hat intensity distribution of the beam profile approached increasingly to a Gaussian intensity distribution. In summary, the focus position change Δf_L of an optical element can be approximately determined over the absorbed laser power P_A for a thin lens with the radius r_L and the focal length f_L based on the material-specific thermal conductivity k_W and the change of the refractive index dn/dT with equation (3) [25].

$$\Delta f_L = -\frac{1}{2} \cdot \frac{P_A \cdot f_L^2}{\pi \cdot k_W \cdot r_L^2} \cdot \frac{dn}{dT} \tag{3}$$

The negative sign illustrates the shift of the focus position along the propagation axis in the direction of the lens. The focal length of a thermally loaded optical element is reduced. The focus position changing Δf_{Optics} of an optical system can be understood as a change in the absolute focal length and can be formally represented by equation (4) with change in temperature ΔT in the center, change in length dL/dT, refractive index change dn/dT, resulting focus f_{OS} of the optical system, lens radius of the last optical element r_{Optics} and thickness d of this optical element [23]. In equation (4) the negative sign is also a shift towards shorter focal lengths of the optical system.

$$\Delta f_{Optics} = -2 \cdot \frac{f_{OS}^2}{r_{Optics}^2} \cdot \left(n(T) \cdot \frac{dL}{dT} + d \cdot \frac{dn}{dT} \right) \cdot \Delta T \tag{4}$$

The conclusion is now, that the machining position of an infrared high power laser spot does not fit anymore to the measured and analyzed position of a green pointing laser spot, such as a combination is used in the high-performance laser remote scanner head of the iLAS. It is absolutely necessary to develop a combined model of the influencing components and parameters, to design a practical and fast correction algorithm supported by real sensor signals and implemented in the laser remote scanner controller unit. Therefor a first model of the main impact factors has been designed and the thermal influences have been simulated.

3. Simulation model of the optical system

3.1. Overview

The first step after an analysis of main impact factors and their effects to the focus of the total lens system is the modeling of the lens system with typical values for lens geometry, material and coating. The modeling of the temperature distribution of a lens to determine the effects of the thermal lens effect is at the forefront. Therefore the FEM modeling software COMSOL Multiphysics is used. From each of the calculated temperature distributions of laser illuminated lenses the thermal focal length of each lens has to be determined and the impacts on the machining process could be estimated. The optical submodels have to be defined and the laser has to be described as heat source. For an optimal solution process a special attention is given to the solver settings of the software COMSOL.

3.2. Geometry setting and mesh adjustment

As basic elements for modeling STEP- and CAD-datasets of the optical systems are available and contain all geometrical data. These sets could be processed into COMSOL-own datasets. The finite elements mesh modeling is a crucial factor for the quality of the simulation environment, the aim fulfillment and the benefit of the calculated solutions. The accuracy of the final results is determined by the fineness of the mesh. If further refinement does not take serious effect to the final results, the mesh fineness is sufficient. Tetrahedron elements with various element sizes build the structure. High temperature gradients and small lenses ($Ø = 50\ mm$) are based on element sizes of maximal $1\ mm$. Lower expecting temperature gradients and bigger lenses ($Ø = 390\ mm$) are characterized through elements with a maximal size of $4\ mm$. In z-direction (beam propagation direction) continuous triangular structures forming the border area of a lens. Figure 2 exemplifies the modeling mesh structure of an asphere and of a lens for focus positioning.

Using finite elements a balance between acceptable calculation time and the desired accuracy has to be found in practice. For a sufficient accuracy of the final results the model based calculating times for the calculation of a lens related temperature distribution lie below $t_{cal} = 70\ s$ using COMSOL simulation environment.

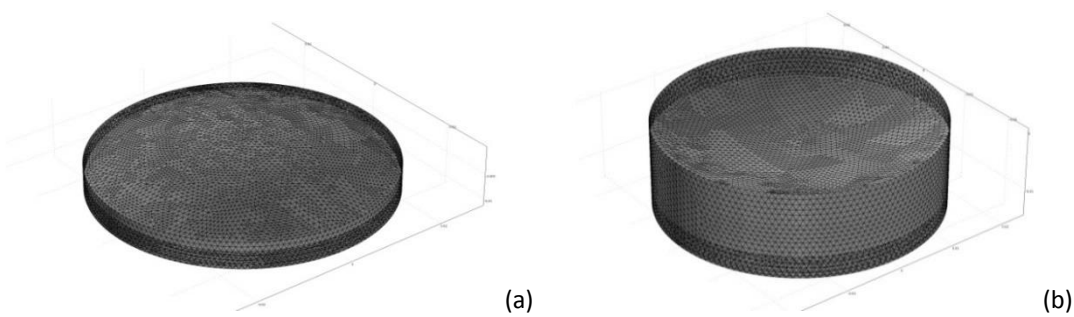

Figure 2: (a) asphere after mesh generation with COMSOL and a maximal element size of 1 mm; (b) lens for focus positioning after mesh generation with COMSOL and a maximal element size of 1 mm

3.3. Material properties

Depending on the application of optical elements manufacturers use different glass types. These differ in the way of manufacturing, in microstructure or degree of purity, such as the homogeneity and the amount of trapped foreign atoms. Exemplary the conventional glass types for high performance laser applications and optical detectors are mentioned. Corning 7980 is a highly purified, amorphous silicon dioxide, which is produced by flame hydrolysis [26]. The colorless quartz glass has a relatively low coefficient of thermal expansion and is available in various sorts and levels of purity [26]. It is the standard for optical laser systems. Suprasil 3001, which is a highly purified quartz glass as well, has a highly optical homogeneity in all three spatial directions and a very low absorption due to a minimal hydroxyl and bubble content [27, 28]. It is more high-graded than Corning 7980, but also more cost intensive. Both sorts of glass are fundamentally suitable for the dimensioning of laser remote scanner system solutions with long focal lengths.

Whereas thermo-physical material properties such as thermal conductivity and specific heat capacity for various sorts of quartz glass diversify marginal there are significant differences in absorption characteristics for the abovementioned materials. Because of the extremely low content of hydroxyl in Suprasil 3001 ($\sim 1\ \mathrm{ppm}$) compared to Corning 7980 ($\sim 800\ \mathrm{ppm}$) results in a significant lower spectral absorption coefficient β for Suprasil 3001 [26, 27]. The spectral absorptions coefficient is still depended on the irradiated wavelength and must be determined experimentally [29]. In literature for Suprasil 3001 a spectral absorption coefficient $\beta = (0{,}3 \pm 0{,}2)\ \mathrm{ppm/cm}$ is listed for a wavelength of $\lambda = 1064\ \mathrm{nm}$ [27]. In comparison, the spectral absorption coefficient β for Corning 7980 is defined as $\beta = 13.5\ \mathrm{ppm/cm}$ [30]. The thermo-physical material properties are shown in table 1. The temperature dependent expansion of the material will be neglected at the first approach.

Table 1: Thermo-physical material properties, refractive index n and its temperature dependence dn/dT for Corning 7980 and Suprasil 3001 [26, 27, 31, 32]

specific heat capacity C_p in $J/(kg \cdot K)$	thermal conductivity κ in $W/(m \cdot K)$	density ρ in kg/m^3	refractive index n	dn/dT in ppm/K
772	1.38	2201	1.449633	9.6

For the compliance of the given values in the simulation model these values have to be passed on the optical elements as constants. Therefore COMSOL provides several module functions. Furthermore the material properties which appear in the general heat equation must be deposited for the simulation of the temperature distribution. The default predefined linear Lagrange elements are adopted in simulation. The reference temperature $\mathrm{T_{Ref}}$ has to be defined to $\mathrm{T_{Ref}} = 20\ ^{\circ}\mathrm{C}$ at instant of time $\mathrm{t} = \mathrm{t_0}$.

3.4. Model of the heat source

The main reason of heating of the lens is the absorbed laser beam power of the lens itself. The absorbed laser beam power of any point of the lens surface respectively of any point within the lens is determined by the intensity distribution of the laser beam on one hand and by the absorption characteristics of the material on the other hand. These effects both together are implemented as stationary heat source in the simulation model. For this purpose, a heat source term is defined as the radiation power, which is converted into heat, per unit of volume [29]. Within the boundary condition of a Gaussian distribution for the intensity of the laser beam [33]

$$I(x,y) = \frac{2 \cdot P}{\pi \cdot R_L^2} \cdot e^{-2 \cdot \frac{x^2+y^2}{R_L^2}} \tag{5}$$

with $\mathrm{R_L}$ as an averaged beam radius across the thickness of the lens, the knowledge of the spectral absorption coefficient β of the material, with a modeled reflectance of 0 and a non-dissipative change of the absorbed laser energy into heat energy results the equation (7) for the heat source term $Q(x,y,z)$ of a coplanar lens from the derivation of the intensity distribution in z-direction [29]

$$I(z) = I(x,y) \cdot e^{-\beta \cdot z} \tag{6}$$

to z and taking equation (5) into account. P is the laser beam power and x, y, z is the orientation of the radiation.

$$Q(x,y,z) = -\beta \cdot \frac{2 \cdot P}{\pi \cdot R_L^2} \cdot e^{-2 \cdot \frac{x^2+y^2}{R_L^2} - \beta \cdot z} \tag{7}$$

As you can see the equation (7) comprised the characteristic laser beam properties as well as the absorption properties of the lens material. Then the source term has to be adapted to the concrete lens shape. For a spherical lens surface the term $-\beta \cdot z$ has to be 0 for all surface points on the laser beam access side.

3.5. Boundary conditions of the optical elements

At last there is the task to force boundary conditions to the modeled elements of the simulation. Beside a lens fixture it is to consider the effective lens surface, which is exposed to the ambient medium. The clamping frames can be observed both insulated to the lens and temperature loaded. Concerning to this the simulation of cooling media at the lens border and their influence can be found out. The heat transfer coefficient h_{conv} is a rate for the thermophysical properties of the ambient medium and its flow rate and declares the convection. So far a passive cooling is modelled. At room temperature $T_{Ref} = 20\ °C$ the heat transfer coefficient h_{conv} reaches values of $h_{conv} = (5 \dots 25)\ W/(m^2 \cdot K^2)$ [34]. The emission ratio ε_{emis} of quartz glass is typically $\varepsilon_{emis} = 0{,}91 \dots 0{,}94$ [34]. An AR coding is still constant designed with an absorption factor of $95\ ppm$.

4. Simulation

4.1. Preconditions

All examinations take place under the limitation of a laser beam source with a beam parameter product $BPP = 18\ mm \cdot mrad$ and a radiated power of $P = 30\ kW$ from a fiber with $d_{fiber} = 300\ \mu m$ and $NA = 0.12$. The Rayleigh length is approximately $z_R = 5.15\ mm$. The magnification ratio of the optical system is designed to a factor of 2:1. The nominal working distance of the laser remote scanner optics is $z_{focus} = 978.83\ mm$. The optical system includes 6 optical elements from $Ø = 50\ mm$ up to $Ø = 390\ mm$ (all are lenses except the protection glass), deflecting mirrors not counted. The first evaluation has been done for the material Corning 7980. As boundary condition of the simulation a heat loss is only possible across the lens surface.

4.2. First results

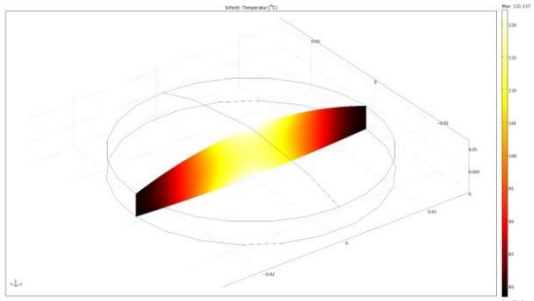

(a)

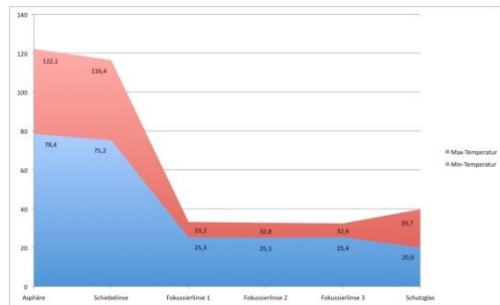

(b)

Figure 3: (a) simulation results for the asphere in a field diagram in °C; (b) maximum and minimum temperature of all 6 optical elements in °C

Based on the simulated temperature field for the optical design of the novel high-performance LRS system, the thermal focal length of each lens can be determined and calculate the propagation of the laser beam by the optical system. This is done both for the initial state with the focal length f_0 and for the steady state with the f_{th} focal length in which acts the thermal lens effect. Comparison of the two focal lengths reflects the thermal focus shift Δf_{Optics}.

Figure 3(a) shows the simulated temperature field of the asphere in a sectional view. It will be appreciated that the temperature gradients along the optical axis can be neglected in comparison to the radial direction. The maximum temperature of the asphere is approximately $\mathrm{T_{as\_max}} = 122\ °\mathrm{C}$ while the minimum temperature is about $\mathrm{T_{as\_min}} = 78\ °\mathrm{C}$. The simulation of the temperature fields of all further lenses shows the same trend qualitatively (figure 3(b)). A difference exists in the maximum temperatures and radial temperature gradients. The temperatures of the asphere and the lens for focus positioning are comparatively high, because in relation to all other lenses the lens radius is only a third.

In a first step, for identification of the thermal focal length the radial gradient of the refraction index n has to be exported from the received simulation data and then a quadratic approximation has to be done. With this result of each lens and the construction data of each lens the thermal focal length of each lens can be identified afterwards. The table 2 shows the determined parameters for all 6 optical elements. Hence can be identified the change in the propagation of the laser beam through the optical system of the LRS.

Table 2: Initial and thermal focus lengths of all 6 optical elements of the high-performance laser remote scanner head for Corning 7980 with $P = 30\ kW$, $AR = 95\ ppm$, $d_{fiber} = 0.300\ mm$, $NA = 0.12$

optical element	f_0 in mm	f_{th} in mm	Δf in mm	$\Delta f / f_0$ in %
asphere	150.00	149.29	- 0.71	- 0.47
focus positioning lens	- 96.61	- 96.59	0.02	0.02
optics set lens 1	926.38	925.28	- 1.10	0.12
optics set lens 2	1008.75	1007.68	- 1.07	0.11
optics set lens 3	925.72	924.77	- 0.95	0.10
protection glass	inf	598831.08	inf	-

In the non-heated status, which is the initial state, the working distance of the laser remote scanner optics is $z_{focus} = 978.83\ mm$ and the focus radius on the workpiece surface is $d_{spot} = 608\ \mu m$. After the simulated steady state (approximately $t_{steady} = 1000$ s) the thermal induct changes of the focal lengths has been calculated (table 2) and the focus shift for the complete optics is about $\Delta f_{Optics} = -10.30\ mm$. The focus distance is reduced and moves from the processing position in direction to the laser remote scanner head. At a Rayleigh length of $z_R = 5.15\ mm$ it means that in the original focus level now exists a laser beam diameter of $d_{spot\_th} = 1360\ \mu m$. According to the diameter that is a magnification by a factor of ≈ 2.23 and thereby a decrease of the intensity in the center of the focus by a factor of 5 respectively a reduction of $80\ \%$. This reduction of intensity is for most laser manufacturing processes not acceptable.

5. Conclusion

In this paper a new high-performance laser remote welding head was presented. It is the first system stereo-vision guided for high power laser applications acting with two different wavelengths for measuring and manufacturing tasks. A special optical system has been developed. At high power systems thermal focal shift takes place. To analyze the impact of the focal shift to industrial manufacturing tasks a first basic simulation model of the optics has been designed. The results show that usual beam emitting duty cycles up to $60\ s$ cause a focal shift for the complete optics of about $\Delta f_{Optics} = -10.30\ mm$ and a loss of $80\ \%$ of laser intensity at the original focus level; this is unacceptable for industrial thin and thick sheet applications. The focus shift has to be tracked and corrected automatically.

Concerning to these results, during the following steps the simulation model has to become more detailed adding all main impact factors, such as thermal deformation and thermal stress, to control the focus position online. It is necessary to transfer the scientific findings into an algorithm implemented in the laser remote scanner controller unit and it is necessary to support the model by real sensor signals. This is the next performance step of the developed laser remote scanner solution by the iLAS in automation for many brilliant high power laser applications using laser remote scanner techniques, especially industrial issues with high accuracy requirements.

Acknowledgements

Parts of the results presented in this paper were generated within the project QuInLas, which was funded and kindly supported by the German Federal Ministry for Economic Affairs and Energy (BMWi) and the Projektträger Jülich (PTJ). The authors acknowledge P. Witte for his work in modeling the simulation environment and in experimental analyzes. Furthermore the authors thank N. Bendig, A. Dittrich, S. Pfau and M. Hoffer for success of the paper.

References

[1] Grupp, M.; Seefeld, T.; Vollertsen, F.: Laser beam welding with scanner. Bremer Institut für angewandte Strahltechnik GmbH. Second International WLT-Conference on Lasers in Manufacturing, München, 2003.

[2] Rippl, P.: Remote-Schweißen mit dem Robot PFO und KUKA Robo-SCAN – Herausforderung und Chancen. EALA – European Automotive Laser Applications 2005. 6th European Expert Conference, Bad Nauheim, Germany, 2005.

[3] Emmelmann, C.; Kirchhoff, M.: Neuartige Strahlführung und -formung für die Laser-Remote-Schweiß-Bearbeitung; Die Verbindungsspezialisten Basel 2007, Düsseldorf 2007.

[4] Oefele, F.: Remote laser-welding of fillet welds – The new Mini doors. EALA – European Automotive Laser Applications 2014. 15th European Expert Conference, Bad Nauheim, Germany, 2014.

[5] Tsoukantas, G.; Stournaras, A.; Chryssolouris, G.; Salonitis, K.; Stavropoulos, P.: On optical design limitations of generalized two-mirror remote beam delivery laser systems: the case of remote welding. The International Journal of Advanced Manufacturing Technology 32 (2007) 9-10, S. 932-941, 2007.
[6] Bergmann, U.: Vereint Schnelligkeit und Flexibilität: Das Remoteschweißen mit dem Laserstrahl (Teil 2). Der Praktiker 61 (2009) 7, S. 234-241, 2009.
[7] Oefele, F.: Remote-Laserstrahlschweißen mit brillanten Laserstrahlquellen. Dissertation. Technische Universität München, München. Institut für Werkzeugmaschinen und Betriebswissenschaften (iwb). 2012.
[8] Emmelmann, C.; Kirchhoff, M.: Design of a solid state laser remote system of high economic efficiency and of high flexibility for multiple applications. In: Vollertsen, F. et al. (Hrsg.): Proceedings of the Fourth International WLT-Conference on Lasers in Manufacturing, München, 18.-22.06.2007. Stuttgart: AT-Fachverlag GmbH (ISBN: 978-3-00-021449-3), S. 437-443, 2007.
[9] Emmelmann, C.: Grundlagen und Bedeutung der Remoteschweißtechnik. 1. VDI Forum Remoteschweißen, Hamburg, 23.06.2004.
[10] Emmelmann, C.; Stemmann, J.: Highperformance Scanner for Remote Welding with Nd:YAG Lasers. 21st International Congress of Lasers & Electro-Optics, ICALEO, Miama, USA, 2005.
[11] Emmelmann, C. et al.: QuInLas – Qualitätsgerechte 3D Laser-Schweißbearbeitung innovativer Schiffskonstruktionen. Vortrag u. Veröffentlichung zur Statustagung Schifffahrt und Meerestechnik 2012. In: http://www.ptj.de/lw_resource/datapool/_items/item_4243/statustagung20122311_internet.pdf, S. 133 ff, 2012.
[12] Emmelmann, C. et al.: Application of the laser remote welding technology with 3D sensors in ship and civil engineering. Vortrag und Veröffentlichung zur IIW International Conference 2013 on “Automation in Welding”, Essen, 16.-17.09.2013.
[13] Stemmann, J. M.: Remote Welding with Solid State Lasers. Dissertation. Technische Universität Hamburg-Harburg, Hamburg. Institut für Laser- und Anlagensystemtechnik (iLAS). Cuvillier Verlag, Göttingen, 2006.
[14] Wollnack, J: Videometrische Verfahren zur Genauigkeitssteigerung von Industrierobotern, Postdoctoral Dissertation, Department of Materials, Design and Manufacturing at the Technical University of Hamburg-Harburg, Technical University of Hamburg-Harburg, March 2000, Shaker Verlag, 2001.
[15] Wollnack, J: Positions- und Orientierungsbestimmung auf der Basis von Positionsinformationen. Technisches Messen (tm), 06/2002, S. 308-316, 2002.
[16] Wollnack, J.: 3D/6D vision systems in robotics and airplane assembly; Airtec, International Aerospace Supply Fair, Frankfurt, 23-26 October, 2007.
[17] Wollnack, J.: 3D/6D Visionsysteme und Lasermessverfahren in der Robotik und Fertigungstechnik der Luftfahrtindustrie; 2. Fortbildungsseminar, Optische Messtechnik für Anwendungen im Maschinenbau, Universität Karlsruhe Geodätisches Institut, Karlsruhe, 17 Oktober, 2008.
[18] Ondracek, G.: Werkstoffkunde. Leitfaden für Studium und Praxis (ISBN 3-88508-966-1), Expert-Verlag, 2. Aufl., 1986.
[19] Haynes, W. M.: CRC Handbook of Chemistry and Physics. 95. Auflage, 2014-2015. Crc Press (ISBN 978-1-4822-0867-2), 2014.
[20] Kogel-Hollacher, M. et al.: Solutions for lasers with high brightness - a deeper look into processing heads for welding and cutting. In: Laser Institute of America (LIA) Hrsg.: ICALEO - 28th International Congress on applications of lasers and electro-optics (Laser Materials Processing Conference). Orlando, 02.-05.11.2009, S. 146-150. 2009.
[21] Abt, F.; Heß, A.; Dausinger, F.: Focusing of high power single mode laser beams. Proceedings of the Forth International WLT-Conference on Lasers in Manufacturing, S. 321-324, München, 2007.
[22] Märten, O.; Kramer, R.; Schwede, H.; Wolf, S.; Brandl, V.: Fokusanalyse. Charakterisierung von Fokussierungssystemen für Hochleistungslaser mit hoher Strahlqualität (Teil 1). Laser + Photonics 2/2008, S. 48-51.
[23] Wolf, S.; Kramer, R.; Märten, O.; Schwede, H.; Brandl, V.: Temporal Behaviour of Focus Shift with Laser Power. Proceedings of the Fifth International WLT-Conference on Lasers in Manufacturing, S. 287-292, München, 2009.
[24] Reitemeyer, D.; Seefeld, T.; Vollertsen, F.; Bergmann, J. P.: Influences on the laser induced focus shift in high power fiber laser welding. Proceedings of the Fifth International WLT-Conference on Lasers in Manufacturing, S. 293-298, München, 2009.
[25] Miyamoto, I.; Nanba, H.; Maruo, H.: Analysis of thermally induced optical distortion in lens during focusing high-power CO2 laser beam. In: SPIE Hrsg.: CO2 lasers and applications II. Bellingham, Wash.: SPIE 1990 (ISBN: 0819403237), S. 420-429. 1990.
[26] Optics, Semiconductor: HPFS Fused Silica Standard Grade. Corning Semiconductor Optics. Forschungsbericht. 2003.
[27] GmbH, Heraeus Quarzglas: Suprasil 3001 und 3002. Heraeus Quarzglas GmbH. Forschungsbericht.
[28] Takke, R.: Spezialaufträge im All und auf der Erde. Heraeus Quarzglas GmbH. Forschungsbericht. 2009.
[29] Petersen, M.: Lasergenerieren von Metall-Keramik-Verbundwerkstoffen, Dissertation. Technische Universität Hamburg-Harburg, Hamburg. Institut für Laser- und Anlagensystemtechnik (iLAS). Cuvillier Verlag, Göttingen, 2006.
[30] Hild, S.; Lück, H.: Measurement of a low-absorption sample of OHreduced fused silica. 2005.
[31] East, Valley Design: Fused Silica Wafers (Corning 7940 & 7980). In: http://www.valleydesign.com/7940.htm, Abruf: 17.05.2015.
[32] GmbH, Heraeus Quarzglas: Quarzglas für die Optik - Daten und Eigenschaften. Heraeus Quarzglas GmbH. Forschungsbericht. 2010.
[33] Saleh, B. E. A.; Teich, M. C.: Grundlagen der Photonik. 2. WILEY-VCH, 2007.
[34] Nelson, P. G.: Thermal Analysis of a 1.5 Meter f/5 Fused Silica Primary Lens For Solar Telescopes. Coronal Solar Magnetism Observatory. Forschungsbericht. 2007.